Dynamic Behavior of the Bering Glacier-Bagley Icefield System During a Surge, and Other Measurements of Alaskan Glaciers with ERS SAR Imagery

Craig S. Lingle	Geophysical Institute, University of Alaska Fairbanks, P.O. Box 757320, Fairbanks, Alaska 99775-7320, USA clingle gi.alaska.edu
Dennis R. Fatland	Geophysical Institute, University of Alaska Fairbanks, P.O. Box 757320, Fairbanks, Alaska 99775-7320, USA
Vera A. Voronina[1]	[1]Now at: Interactive Software Systems, Inc., 7175 West Jefferson Ave., Suite 2500, Denver, Colorado 80235, USA
Kristina Ahlnäs	Geophysical Institute, University of Alaska Fairbanks, P.O. Box 757320, Fairbanks, Alaska 99775-7320, USA
Elena N. Troshina	Geophysical Institute, University of Alaska Fairbanks, P.O. Box 757320, Fairbanks, Alaska 99775-7320, USA

Abstract

ERS-1 SAR imagery has been employed for measurement of the dynamics of Bagley Icefield during a major surge in 1993-'94, measurement of ice velocities on Malaspina Piedmont Glacier during a quiescent phase between surges, and for mapping of snow lines and the position of the terminus of Nabesna Glacier on Mt. Wrangell (a 4,317 m andesitic shield volcano) in the heavily glacierized St. Elias and Wrangell Mountains of Alaska. An overview and summary of results is given. The methods used include interferometry, cross-correlation of sequential images, and digitization of boundaries using terrain-corrected SAR imagery.

Keywords: Glaciology, Alaskan glaciers , Bering/Malaspina Glaciers

1. Introduction

The combined Bagley Icefield and Bering Glacier system (Fig. 1), with an area, including tributaries, of 5,200 km2 and a length of 190 km, constitute the largest and longest glacier system in North America. Bagley Icefield, which is the accumulation area of Bering Glacier, was not recognized as such historically because it was first observed from its eastern end, which forms a broad ice divide at about 2,010 m below the north side of Mt. St. Elias (5,489 m). Nineteenth-century explorers attempting to climb Mt. St. Elias, including Luigi Amedeo, Duke of the Abruzzi, who successfully made the first ascent in 1897, did not recognize that the huge glacier now named Bagley Icefield actually forms the upper reaches of the distant and similarly vast Bering Glacier, which had been named earlier, independently, after observation from the coast. (See Molnia and Post [1995] for a historical summary and the Holocene history of Bering Glacier.)

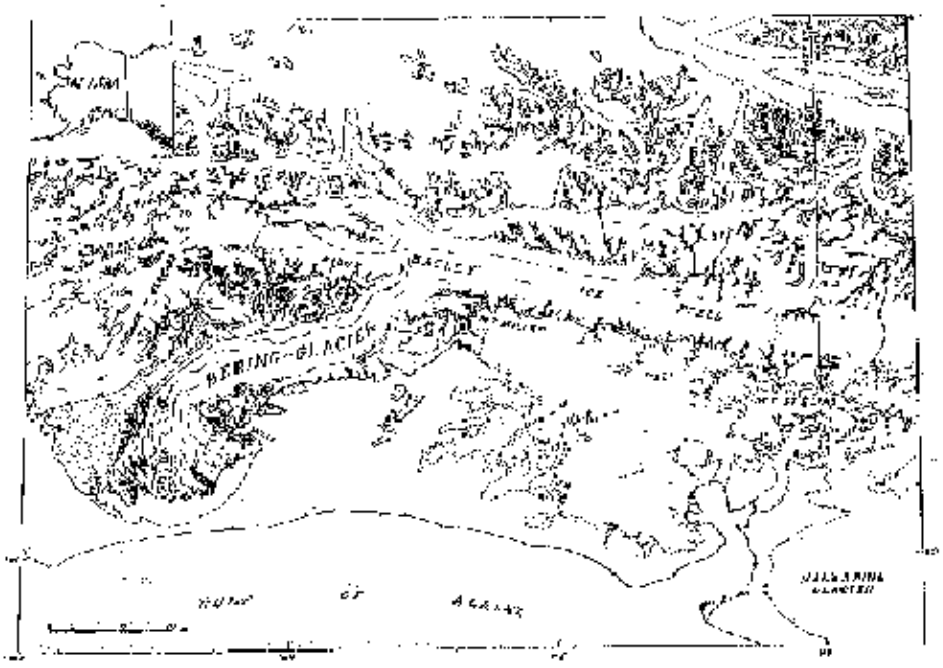

Fig. l . Location of Bering Glacier, Bagley Icefield, and Malaspina Glacier, Alaska, U.S.A. (from Post, 1972).

Bering Glacier surges with a period of approximately 17 to 26 years, with renewed surges or secondary pulses sometimes occurring at shorter intervals (Molnia and Post, 1995). (A glacier surge is a sudden acceleration of flow up to 10 to 100 times

normal which lasts of the order of one to several years, which is often [but not always] accompanied by an advance of the terminus, and which is followed by a period of quiescence lasting of the order of 10 to 100 years. Glacier surges tend to be periodic or quasi-periodic.)

SAR interferometry, based on complex image-pairs acquired during the ERS-1 ice phases, is used to show that by February 1994 the surge which began in spring 1993 and reached the terminus in late-August/early- September 1993 (Roush, 1996) had also propagated up- glacier into Bagley Icefield.

Farther east-on the eastern side of the broad divide which forms the head of the westward-flowing Bagley Icefield- Seward Glacier, flowing east, is the main source feeding Malaspina Glacier, which is a 50 km-wide piedmont glacier terminating, like Bering Glacier, on the Gulf of Alaska coast. We employ the method of cross-correlation of sequential ERS-1 images to measure the surface velocities on this large expanse of ice. In addition, an interferogram synthesized from an image-pair with a 1-day time separation-acquired during the ERS-1 and ERS-2 Tandem Mission-is used to illustrate the motion of Malaspina Glacier.

Finally, the utility of terrain-corrected SAR imagery for digitizing late-summer snow lines and the positions of glacier termini, which are closely related to glacier mass balance, is illustrated on Mt. Wrangell's 85 km-long Nabesna Glacier. Mt. Wrangell (62° N, 144°W, 4,317 m) and Nabesna Glacier are chosen because the gentle slopes and relatively high summit altitude of this andesitic shield volcano result in a complete range of facies that are easily-observable with spaceborne SAR, from the bare ice of the ablation area to the wet snow facies above the snow line, the percolation facies at higher altitudes, and the dry snow facies within the summit caldera (Benson and others, 1996).

2. Upstream Propagation of the Bering Glacier Surge

The first evidence of the 1993-'94 surge of Bering Glacier was noted far below Bagley Icefield in the lower ablation area, at a point roughly 22 km up-glacier from the terminus, in a SAR image acquired 30 April 1993 (Lingle and others, 1994; Roush, 1996). During the course of a small airplane flight on 19 June 1993 carried out as part of a field program, abundant evidence of surging was seen on the lower glacier, but this gradually faded out upstream and no evidence of surging was seen relatively high up on Bering Glacier, still within the ablation area but below Bagley Icefield; that is, roughly 75 km up-glacier from the terminus (Lingle and others, 1993).

Fig.2 is an interferogram synthesized from an image-pair acquired by ERS-1 during January 1992, during the First Ice Phase. The 2 images were separated by 3 days along an exact repeat orbit. The interference fringes represent both the effects of topography and ice motion; however, the ice motion signal is dominant (e.g. Goldstein et al., 1993; Zebker et al., 1994). Bagley Icefield (bright fringes) enters from right, flowing right to left. Bering Glacier (decorrelated due to faster ice motion, no fringes) flows toward the lower-left corner. West Bagley Icefield (mostly decorrelated) enters from left-center, flowing left-to-right. Tana Glacier (bright fringes) flows toward upper left. The area left of center is a multiple divide, with the dominant flow entering from Bagley Icefield (lower-right) and continuing down Bering Glacier, which leaves Fig. 2 at lower-left. This interferogram represents the state of flow, 'somewhat contaminated' by the effects of topography, at the multiple flow-divide above Bering Glacier, prior to the onset of the 1993-'94 surge. (A detailed analysis of the flow of West Bagley Icefield, with differential SAR interferometry used to separate the effects of ice motion and topography, is in preparation [Fatland and Lingle]; also Fatland and Lingle, 1994.)

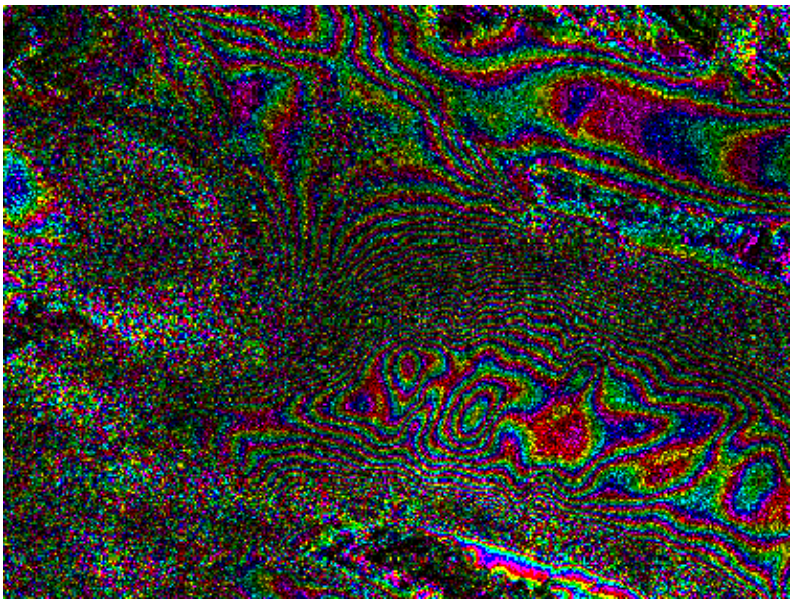

Fig. 2. Flow divide where Bering Glacier descends from Bagley Icefield: January 1992, pre-surge. SAR images in Figs. 2-6 are ©ESA, 1992-96.

Fig.3 is an interferogram synthesized from an image-pair acquired 4 and 7 February 1994 from an exact-repeat orbit, during the Second Ice Phase, while the surge of Bering Glacier was in full progress. As in Fig. 2, the fringes represent the effects of both topography and ice motion, with the motion signal dominant. Although the glacier topography is approximately the same in both figures, the topographic contribution to the phase is not the same because of the differing baselines. Due to dominance of the motion signal, however, the change in the fringes can be taken, qualitatively, as indicating the acceleration of flow caused by the surge. The greatly-increased decorrelation of Bagley Icefield, right of center, shows that the surge propagated upglacier into the icefield, as well as down-glacier to the terminus. (The evidence for the latter, which was inescapable-indeed, dramatic-was observed independently, and is not discussed here.) The effect of increased shearing along the sides of Bagley Icefield is shown by increased decorrelation near the valley walls. Fig. 3 also shows more closely-spaced fringes on Tana Glacier (a distributary), indicating increased flow rates.

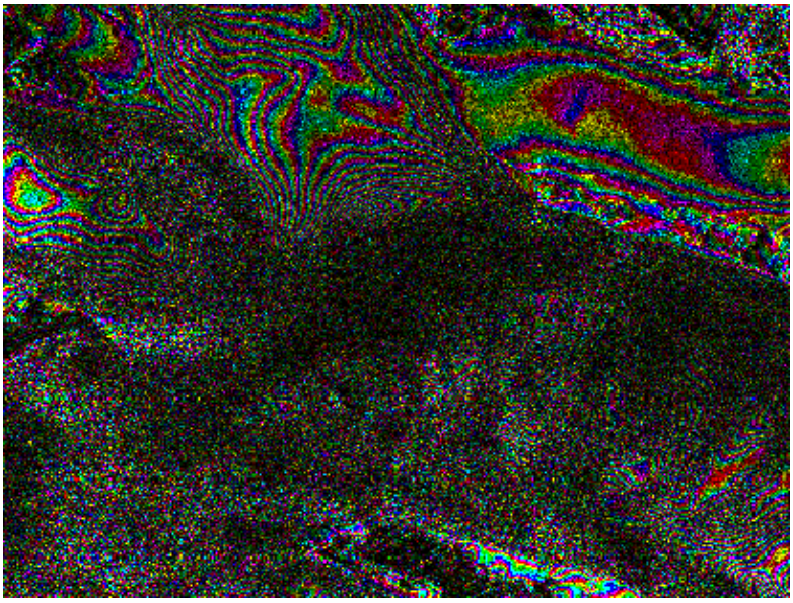

Fig.3. Flow divide where Bering Glacier descends from Bagley Icefield: February 1994, during surge.

3. Velocities on Malaspina Glacier during a Quiescent Phase

Malaspina Piedmont Glacier is fed primarily by Seward Glacier and, with a diameter of approximately 50 km, it has long been known both for its size and the immense folded moraines, clearly recognizable in satellite imagery, that form striking patterns on its surface. The moraines move with the flow of the ice, which suggested that a statistical technique based on cross-correlation of sequential SAR images, analogous to that used by Bindschadler and Scambos (1991) for measurement of a West Antarctic ice stream using Landsat imagery, might be suitable for measurement of surface velocities on Malaspina Glacier using SAR.

Full-resolution SAR images acquired by ERS-1 on 29 June 1992 and 14 June 1993 from an exact repeat orbit during the April 1992 to December 1993 35-day orbit cycle were employed. Images acquired during the same season- preferably, the same month-were considered necessary, to minimize decorrelation caused by seasonal effects. The images were radiometrically calibrated, to a range of - 25.0 to 0.0 db.

Measurement of the misregistration between the two images was made to within sub-pixel accuracy, using cross-correlation of a set of square reference areas defined on the fixed topography around the glacier. A full cross-correlation between the two images was then carried out. Over moving ice the apparent displacements included the movement of the glacier surface, misregistration of the 2 images, and (possibly) the effects of other factors contributing to false correlation. For use in eliminating the latter, a minimum 'strength of correlation' was required. The cross-correlation was also carried out in reverse. If the apparent displacements resulting from both forward and reverse correlation were consistent, the displacement was accepted and defined as the average of the 2 cases.

The component of displacement caused by misregistration was then subtracted from the total apparent displacement. Finally, to be considered acceptable a vector had to show at least 3 pixels (37.5 m) of displacement, equivalent to a mean velocity of 37.6 m/yr. Three pixels is slightly greater than the 30 m resolution of the imagery. The few remaining displacement vectors that appeared to be spurious were edited by hand.

The measured ice displacements, converted to velocity, are shown in Fig. 4-note scale in lower left corner. The vast majority of successful measurements were on the eastern side of Malaspina Glacier where the large folded moraines form distinctive patterns. The maximum velocity vector about 5.3 km down-flow from Seward Glacier represents ice movement at about 420 m/yr.

The results (Fig. 4) were found to be roughly consistent with earlier measurements of velocity, made over a period of 10 years by Krirnmel and Meier (1975), in several areas where direct comparisons could be made. An implication is that the Seward-Malaspina system did not surge during 1962-'72, the time interval of the earlier measurements, nor did it surge during the 1992-'93 interval of the SAR- derived measurements.

Subsequently, a complex image-pair covering Malaspina Glacier was identified, acquired on 22 and 23 January 1996 during the ERS-1 and -2 Tandem Mission. The pair proved to have high coherence, and yielded an excellent interferogram (Fig. 5). The image-pair has been co-registered only 'by hand,' to within an accuracy of about 1 pixel. No attempt has been made to separate the surface-motion and topographic contributions to the interferometric phase. (The perpendicular component of the baseline was 169 m, so the topographic contribution to phase is significant.) The two effects form similar spatial patterns, however. That is, the glacier is convex-up, with the highest surface elevations (about 600 m) and also the highest ice velocities at the outlet of Seward Glacier (top center). The ice flows generally down the surface gradient, spreading radially toward the margins, which are within about 30 m of sea level (at bottom). The fringe pattern thus illustrates both the radial flow, as illustrated by the vector field in Fig.4, with tightly-spaced fringes representing high ice velocities in the mouth of Seward Glacier, and also the surface topography of the lobe.

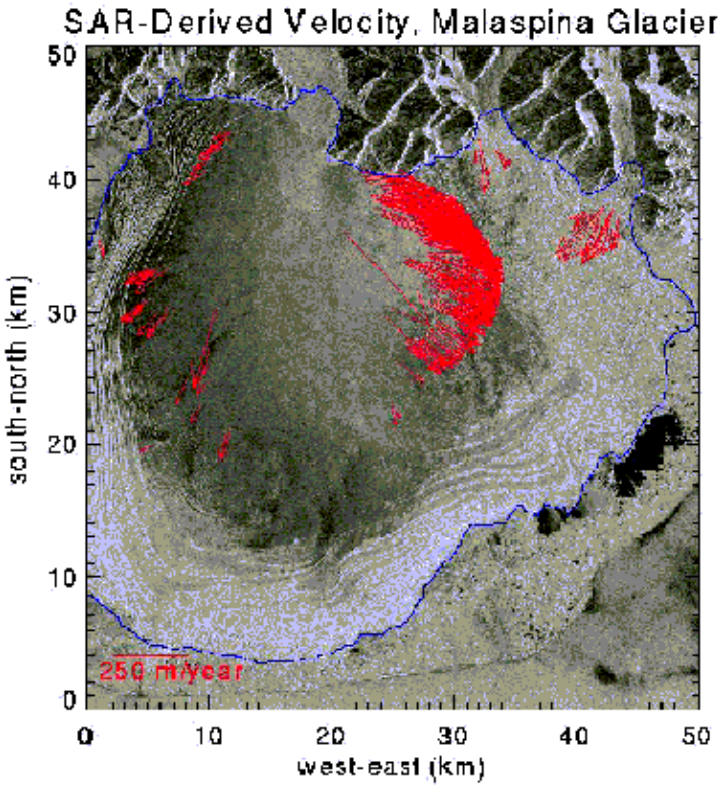

Fig.4. Ice velocities on Malaspina Glacier, measured with cross-correlation of 2 SAR images aquired 29 June 1992 and 14 June 1993.

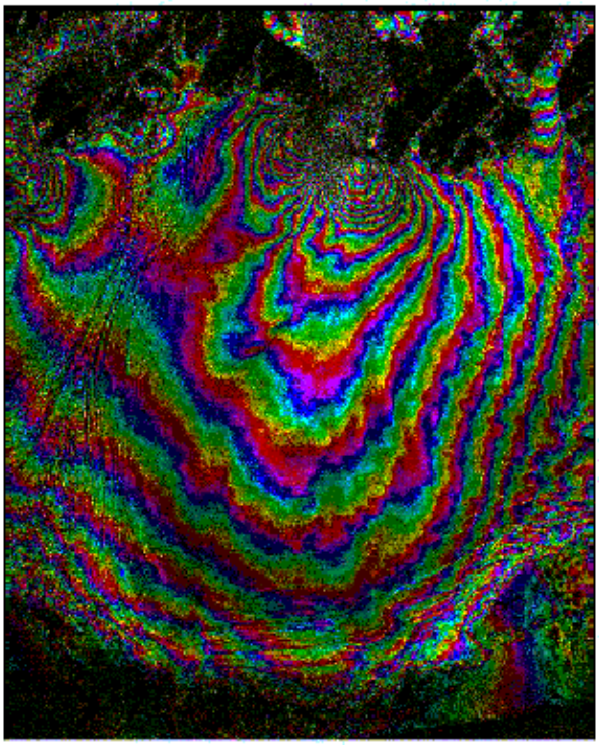

Fig.5. Interferogram of Malaspina Glacier, from ERS-1 and -2 Tandem Mission data. Images were aquired 22 and 23 January 1996.

4. Snow Line and Terminus Positions Digitized on Mt. Wrangell

Fig. 6 is a terrain-corrected (see, e.g., Wivell and others, 1992) SAR image acquired by ERS-1 on 30 December 1992, showing Mt. Wrangell (4,317 m, at left-center) and Nabesna Glacier, which are located about 200 km north-northwest of the Bering Glacier

piedmont lobe shown in Fig. l. Nabesna Glacier is 85 km long, from the crater rim of Mt. Wrangell to its terminus at upper right. Its width, in the lower reaches at right to upper-right, is about 5 km. Fig. 6 shows the clear nature of the boundary (below center) between the ablation area and the refrozen firn of the wet snow facies, which permits straightforward digitization of the late-summer snow lines on Alaskan glaciers using winter SAR imagery. This is the case because the cold, dry snow of winter is transparent to the C-band SAR. Beneath the winter snow cover, the ablation area appears dark because of the specular nature of the ice. Above the snow line, the refrozen firn backscatters brightly and appears almost white (or, in Fig. 6, pinkish-white).

Prior to terrain correction, the digital elevation model (DEM) of Alaska (U.S. Geological Survey, 1990) was interpolated from 90 m to 30 m, using the optimum interpolation method of kriging (e.g., Isaaks and Srivastava, 1989). The terrain-corrected full-resolution image thus has a pixel size of 30 m, and is tightly coupled to the DEM. The late-summer snow line on upper Nabesna Glacier is the sharply-defined white/dark boundary below the center of the image. The mean position of this snow line was found to be lat. 61.8783° N, long. 143.445° W. The corresponding mean position in universal transverse mercator (UTM) coordinates, also read from the DEM, was found to be 6,862,842 northing (m), 371,438 easting (m).

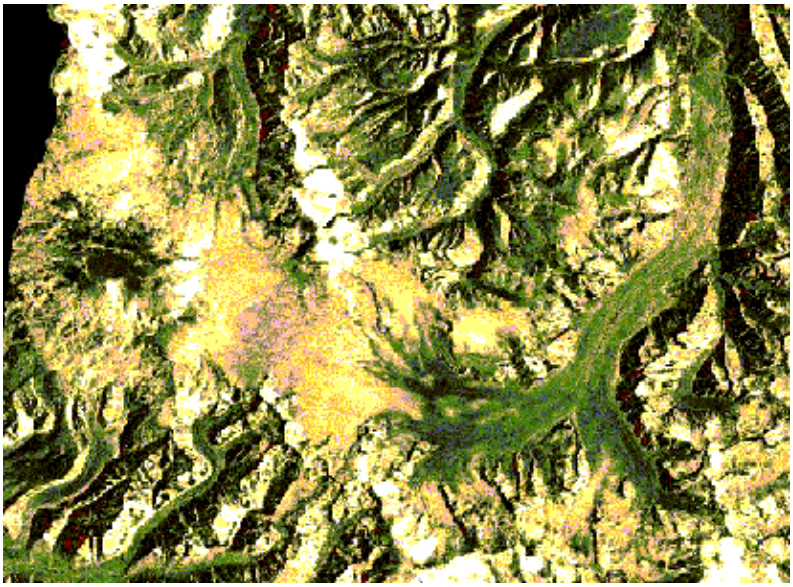

Fig.6. Terrain-corrected SAR image of Mt. Wrangell (left-center) and Nabesna Glacier, flowing from left-center to upper-right, aquired 30 December 1992.

The terminus of Nabesna Glacier (upper right in Fig. 6) was found to be more clearly identified in a SAR image (not shown) acquired by ERS-1 on 10 September 1993, and was similarly digitized using the terrain-corrected version of that image. The mean position of the terminus was found to be lat. 62.1888° N, long. 142.898° W. The corresponding mean position in UTM coordinates was found to be 6,896,463 northing (m),401,210 easting (m).

5. Summary

Satellite SAR imagery has been found to be suitable for measurement of velocities and changes in velocity on Alaskan glaciers using interferometry and/or cross-correlation of sequential images, and measurement of the positions of features related to glacier mass balance, such as snow lines and termini.

Acknowledgments

This work was supported by NSF grant OPP-9319873, by the Cray Research, Inc., 1994-'96 University Research and Development Grant Program, by NASA grant NAGW-4930, and by National Park Service Cooperative Agreement CA 9700-5-9022 to C.S. Lingle, and by a NASA-Alaska SAR Facility research assistantship to D.R. Fatland. Computational support was provided by the Arctic Region Supercomputing Center, University of Alaska Fairbanks.

References

Benson, C.S., C.S. Lingle, and K. Ahlnas. 1996:
Glacier facies on Mt. Wrangell, examined by SAR imagery. *Eos Trans. AGU*, **77**(46), Fall Meet. Suppl., p. F195.

Bindschadler, R.A., and T.A. Scambos. 1991:
Satellite-image-derived velocity field of an Antarctic ice stream. *Science,* **252**, pp. 242-246.

Fatland, D.R., and C.S. Lingle. 1994:
The surface velocity field on Bagley Icefield, Alaska, before and during the 1993-'94 surge of Bering Glacier, from ERS-1 SAR interferometry. *Eos Trans. AGU Fall Meet Suppl.,* **75**(44), p. 62.

Fatland, D.R., and C.S. Lingle, In preparation:
Analysis of the 1993-'95 Bering Glacier surge using differential SAR interferometry.

Golstein, R.M., H. Engelhardt, B. Kamb, and R.M. Frolich. 1993:
Satellite radar interferometry for monitoring ice sheet motion: Application to an Antarctic ice stream. *Science*, **262**, pp. 1525-1530.

Isaaks, E.H., and Srivastava, R.M. 1989:
Applied Geostatistics, Oxford University Press, New York.

Krimmel, R.M., and M.F. Meier. 1975:
Glacier applications of ERTS images., *J. Glaciol.,* **15**(73), pp.391-402.

Lingle, C.S., A. Post, U.C. Herzfeld, BF. Molnia, R.M. Krimmel, and J.J. Roush, 1993:
Bering Glacier surge and iceberg-calving mechanism at Vitus Lake, Alaska, U.S.A. *J. Glaciol.,* **39**(133), pp. 722-727.

Lingle, C.S., J.J. Roush, and D.R. Fatland, 1994:
Time of onset of the 1993-'94 surge of Bering Glacier, Alaska, and effect on iceberg calving of surge arrival at the terminus. *Eos Trans. AGU, Fall. Meet. Suppl*., **75**(44), p. 64.

Molnia, B.F., and A. Post. 1995:
Holocene history of Bering Glacier, Alaska: A prelude to the 1993-1994 surge. *Physical Geography*, **16**(2), pp. 87-117.

Post, A. 1972:
Periodic surge origin of folded